Final Report for "High Latitude Climate Modeling: ARM Takes Us Beyond Case Studies" (DE-SC0001239) for 8/1/2009 through 1/31/2013

1. DOE Award Number: DE-SC0001239.
Name of Recipient: Scripps Institution of Oceanography, University of California, San Diego.
Project Title: High Latitude Climate Modeling: ARM Takes Us Beyond Case Studies
Name of Principal Investigator: Lynn M. Russell (Scripps-UCSD).
Co-PI: Dan Lubin (Scripps-UCSD).
Collaborators: Andy Vogelman (BNL).

2. There are no authorized distribution limitation notices.

3. Executive Summary

Description of the Project: The main thrust of this project was to devise a method by which the majority of North Slope of Alaska (NSA) meteorological and radiometric data, collected on a daily basis, could be used to evaluate and improve global climate model (GCM) simulations and their parameterizations, particularly for cloud microphysics. Although the standard ARM Program sensors for a less complete suite of instruments for cloud and aerosol studies than the instruments on an intensive field program such as the 2008 Indirect and Semi-Direct Aerosol Campaign (ISDAC), the advantage they offer lies in the long time base and large volume of data that covers a wide range of meteorological and climatological conditions. The challenge has been devising a method to interpret the NSA data in a practical way, so that a wide variety of meteorological conditions in all seasons can be examined with climate models. If successful, climate modelers would have a robust alternative to the usual “case study” approach (i.e., from intensive field programs only) for testing and evaluating their parameterizations’ performance.

How this Research Adds to the Understanding of Climate Change: Understanding climate change on regional scales requires a broad scientific consideration of anthropogenic influences that goes beyond greenhouse gas emissions to also include aerosol-induced changes in cloud properties. For instance, it is now clear that on small scales, human-induced aerosol plumes can exert microclimatic radiative and hydrologic forcing that rivals that of greenhouse gas–forced warming. This project has made significant scientific progress by investigating what causes successive versions of climate models continue to exhibit errors in cloud amount, cloud microphysical and radiative properties, precipitation, and radiation balance, as compared with observations and, in particular, in Arctic regions. To find out what is going wrong, we have tested the models' cloud representation over the full range of meteorological conditions found in the Arctic using the ARM North Slope of Alaska (NSA) data.

4. Comparison of the Actual Accomplishments with the Objectives

The *project objectives* were to improve scientific models about the potential response of the Earth's climate to increased greenhouse gas levels by assembling datasets at high temporal resolution in order to:

(1) Use active sensor data and cloud microphysical retrievals from selected radiometric data to validate model simulations of cloud microphysics, involving detailed diagnostic testing of individual components within current cloud microphysical models, leading to suggestions for specific improvements to each component where necessary. Our data set compilation followed two approaches, which are described in detail in Mülmenstädt et al. (2012):
   a. Defining a three-axis climatological ensemble, based on Pacific sector climatology, into which we will sort all suitable cases from the NSA data.
   b. Using k-means clustering in an attempt to let meteorological categories emerge from the data without a priori sorting.

(2) Use unique ARM spectral radiometric data to validate the surface radiation budget predictions that result from the cloud microphysical simulations. For radiometric closure, we made novel use of the AERI Channel 2 data and analyzed ground-based spectroradiometer from the recent successful Indirect and Semi-Direct Aerosol Campaign (ISDAC). The results of these analyses are described in Mülmenstädt et al. (2013), where our overall strategy for this testing and evaluation was to
   a. Determine how realistically the full model simulates the cloud and radiation field in detail (by keeping track of each important microphysical parameter).
   b. Disable the various components of the model to note which components are primarily responsible for the model's performance.
   c. Identify modifications to the microphysics to that improve model realism.

5. Summary of Project Activities

Our approach to organizing the 11-plus years of NSA data was to use *k*-means clustering to naturally sort the data into clusters representing prevailing synoptic conditions. As a check, we used manual analysis of National Center of Environmental Prediction (NCEP) reanalysis data on a subset of the time series comprising two representative years. The *k*-means clustering was applied to the NSA meteorological data, while the various NSA cloud sensor data were left alone to later determine if emerging clustering patterns corresponded to genuine differences in cloud properties. The method yielded four stable categories, which corresponded statistically to prevailing synoptic regimes as shown in Table 1. Figure 1 illustrates how measured cloud properties correspond to the clustering categories.

This method allows the majority of NSA measurements to be sorted into the four categories, and each category then comprises an ensemble of measurements against which GCM simulations can be tested and evaluated. The variance in measured cloud properties within each category describes the natural variability within a given prevailing synoptic condition and season. A paper describing this method has been published in the *Journal of Climate* (Mülmenstädt et al., 2012).

We then carried out a demonstration study, applying the clustering method to the NCAR cloud microphysical models contained in the widely-used Weather Research and Forecasting (WRF) regional climate model, set up to run on a geographic area containing Northern Alaska and the Southern Beaufort and Chuckchi Seas, and centered on the NSA site. We ran single-moment and double-moment cloud microphysical models in WRF, initialized by daily NCEP reanalysis data, for all 11 years corresponding to the NSA data. We then sorted the model output into the categories derived from the *k*-means clustering. This procedure indicates where the model performs well for a given cloud or radiation property and where it generates discrepancies when compared with the ensemble data. Examples for liquid water content and downwelling longwave radiation are shown in Figure 2. Determination of these discrepancies versus ensemble data then provides insight for the modelers as to what processes in their parameterizations may need refinement. A manuscript based on this demonstration study is in preparation for the *Journal of Climate* (Mülmenstädt et al., 2013).

Table 1. Correlation table between synoptic and local classification. Cell entries give the percentage of days in each cluster on which a given synoptic system was identified in a representative 2-yr time period (2000 and 2009). Columns are further grouped by location (North or South of the NSA site) and type (high or low pressure) of the synoptic system. For each local category, the most common synoptic categories are identified, and the fraction of days accounted for by these categories is given in bold face. Cluster (category) 1 corresponds to high pressure systems to the North; cluster 2 corresponds to low pressure systems to the North; cluster 3 corresponds to high pressure systems to the North and low pressure systems to the South, both causing easterly 850-hPa winds at the NSA site; and cluster 4 corresponds to low pressure systems in the Siberian, Chukchi, and Bering Sea with predominantly southerly to westerly flow. From Mülmenstädt et al. (2012).

	Low pressure			High pressure		
	North		South	North		South
Cluster	Beaufort Sea and Central Arctic Ocean low (AOL)	Siberian and Chukchi Seas low (SL)	Aleutian and Bering Sea low (ABL)	Arctic Ocean high (AOH)	Siberian high (SH)	Aleutian and Bering Sea high (ABH)
1	5	7	11	47	26	4
				Combined: 73		
2	48	24	13	1	11	2
	Combined: 72					
3	7	3	45	29	16	1
			Combined: 74			
4	12	24	27	19	8	11
		Combined: 51				

Also part of this work plan was the analysis of ARM Indirect and Semi-Direct Aerosol Campaign (ISDAC) Data. Here we made considerable progress. We focused on the ground-based shortwave ASD (Inc.) spectroradiometer data collected from NSA during April-May, 2008. We found that it is possible to retrieve an effective cloud optical depth from surface flux measurements around 1000 nm, where there is enough decrease in the snow surface albedo to allow sensitivity in the flux to cloud optical depth. With these optical depth retrievals, we the performed for each measurement a simulation of the theoretical surface spectral flux that would prevail under clean-air conditions, the same solar zenith angle and surface condition, and a liquid water cloud with effective radius 11 microns having the same optical depth as retrieved. In the near-IR windows (1.6 and 2.2 microns), we find that the surface spectral flux is highly sensitive to the cloud thermodynamic phase, with the presence of only a little ice in the cloud being sufficient to cause excess attenuation of the surface flux up to 5-10 Watts per square meter. Furthermore, we found this "supplemental near-IR absorption," A_{si}, due to ice in most of our data from April-May, 2010. A manuscript was published in the ISDAC special issue of *Journal of Geophysical Research – Atmospheres* (Lubin and Vogelmann, 2011).

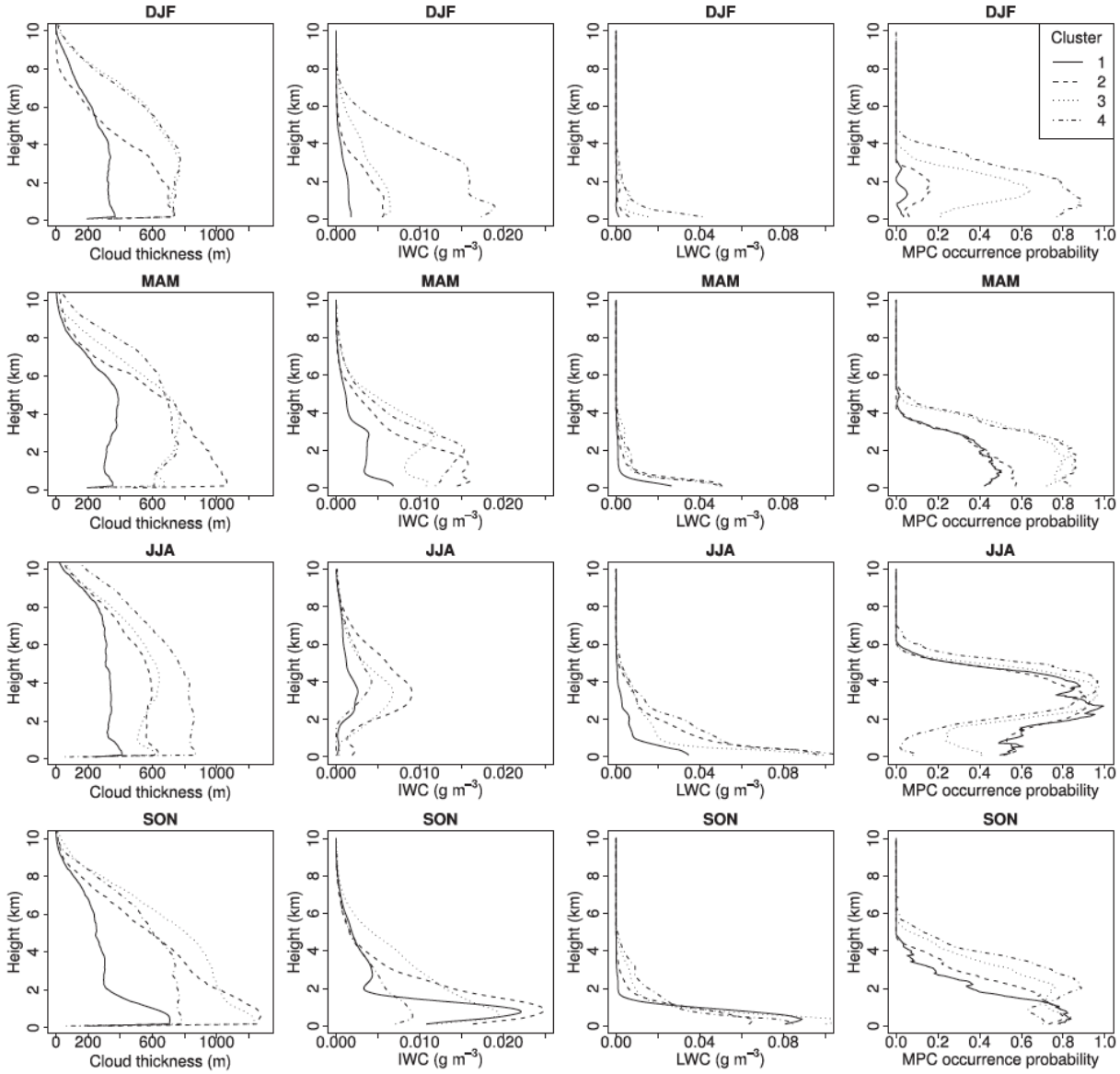

Figure 1. Vertical profiles of average cloud thickness, ice water content (IWC), liquid water content (LWC), and probability of occurrence of mixed-phase cloud (MPC). All probabilities are separately composited by season (rows) and meteorological regime/cluster (line style). Cloud thickness is reconstructed from the ARM ARSCL data product. The remaining quantities are reconstructed from Microbase. The presence of mixed-phase cloud is estimated by testing for simultaneous nonzero LWC and IWC at the same height, and is conditional upon the presence of cloud of any kind. From Mülmenstädt et al. (2012).

Having found a way to discriminate between liquid water and mixed phase Arctic stratiform clouds, we then worked on a method to retrieve cloud droplet effective radius r_e and liquid water path *LWP* in the former. ASD spectroradiometer measurements in the near-IR 1028 nm and 1.6-μm windows enable a direct retrieval of r_e. Given τ_c and

r_e, the cloud liquid-water path, *LWP*, can be obtained through the relationship, $\tau_c = (3/2)(LWP/\rho_x r_e)$, where ρ_x is the density of

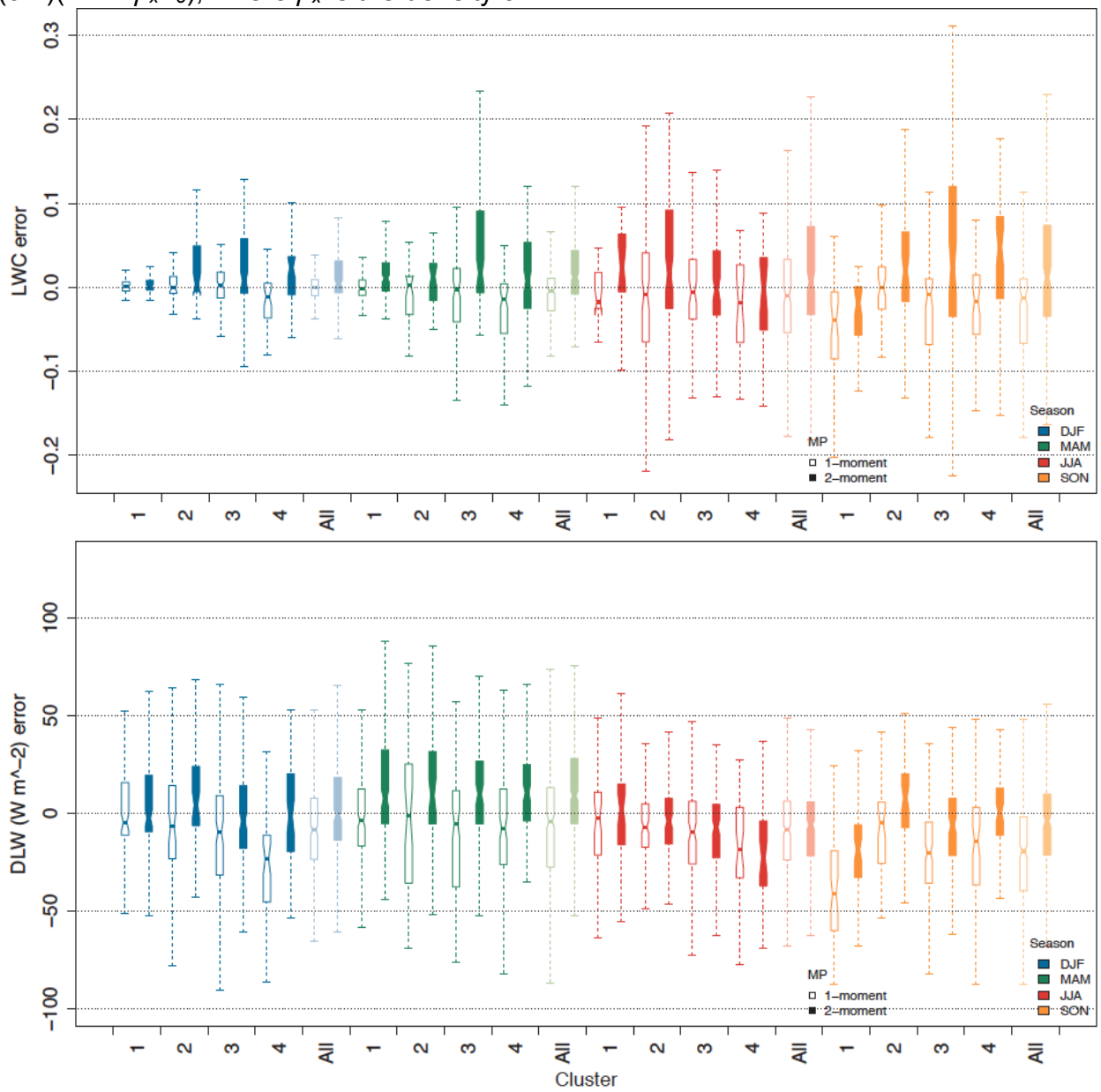

Figure 2. Box and whisker plots showing error in WRF performance when simulating cloud liquid water path (top) and downwelling longwave radiation (bottom) as compared with the *k*-means clustering ensemble data of Mülmenstädt et al. (2012), also broken out by season. Open (solid) symbols pertain to the single- (double-) moment cloud microphysical parameterization.

water; this yields an internally consistent set of τ_c, r_e, and *LWP* for the same field of view (FOV). We made progress with an algorithm for Arctic liquid water clouds as identified using the supplemental ice absorption A_{si} discussed in Lubin and Vogelmann (2011). This algorithm is applied to all spectra having $A_{si} < 5\%$ (little or no ice absorption at 1.6 μm), and obtained under overcast conditions with cloud base height below 1000 m and

total cloud thickness < 3000 m. We perform a weighted least-squares fit to the irradiances measured at 1028, 1534, and 1593 nm, using a discrete-ordinates radiative transfer model. The 1028 nm wavelength region samples a part of the conservative scattering regime for cloud droplets and cloud ice particles, in which the surface albedo (0.72) is smaller than at visible wavelengths (>0.95), thereby allowing more sensitivity to cloud optical depth in Arctic irradiance data. The other two wavelengths sample part of the near-IR (1.6 μm) window in which liquid water clouds are spectrally distinct from ice or mixed-phase clouds, as discussed above.

Figure 3 shows histograms of the retrieved cloud optical depth and effective radius. Here the results are sorted into two categories of cloud thickness. There is a slight tendency for larger optical depths for the geometrically thicker clouds. There is a noticeable tendency toward larger r_e for thicker clouds. This is understandable as r_e generally increases with altitude in liquid water stratiform clouds. Most of these predominantly liquid water clouds were sampled in May 2008, rather than April. Consequently, aerosol CN concentrations were relatively low, and this is consistent with the relatively large mode values of r_e that appear in Figure 3. We demonstrate that the retrievals are physically realistic and stable, as shown in Figure 4. This figure shows that there is no residual dependence on solar zenith angle, nor is there any residual dependence of retrieved r_e on τ_c. We notice that many retrievals of r_e (~30 μm) are probably spurious; they are poorer fits to the radiative transfer calculations (Figure 4d) and occur at lowest sun elevation (Figure 4b), and for very small retrieved τ_c (Figure 4c). Also, for r_e > ~20 μm, we can expect drizzle formation in marine stratocumulus, which was not evident in the data analyzed herein – another clue that these larger retrieved r_e might be spurious. These spurious retrievals - a small fraction (<5%) of the total - are probably spectra obtained under very tenuous clouds or other conditions for which a plane-parallel radiative transfer model does not apply very well. A manuscript discussing this Arctic liquid water cloud retrieval method is in preparation for the *Journal of Atmospheric and Oceanic Technology* (Lubin and Vogelmann, 2013).

We also addressed an issue with the ASD spectroradiometer performance under clear skies. Our initial attempts to derive aerosol optical thickness from the ISDAC data were unsuccessful, because of an inability to match data collected under clean-air and cloud-free conditions with radiative transfer model calculations. We determined that this was due to measurement error in the spectroradiometer's cosine collector. Specifically, when the collector is unevenly illuminated as the direct solar beam changes in elevation angle, imperfections in the collector's cosine response will be magnified, particularly at low Sun elevations. Under diffuse radiation (i.e., stratus clouds), this is not a factor, and our cloudy-sky data interpretation is unaffected. However, to eventually make use of the ASD spectroradiometer data collected under clear skies, we had the instrument's cosine response accurately evaluated by a local San Diego company, Biospherical Instruments (BSI, Inc.) that has an optical bench set up for this purpose.

The directional response of the ASD instrument was characterized with BSI's Directional Response Tester (DRT) for in-air instruments. Figure 5 shows a sketch of a DRT. It consists of a computer-controlled rotary table and hardware to mount the

instruments such that the axis of rotation is tangent to the center of the instrument's diffuser (the white piece located in the center of the collector of the ASD system). The mounting hardware also allows to manually turn the collector around its optical axis to characterize the directional response as a function of azimuth angle. An FEL 1000 Watt tungsten halogen lamp served as the light source. The lamp was mounted at 165 cm from the diffuser. Prior to measuring the directional response, all system components were aligned with a laser. The laser is mounted behind the lamp and its beam is

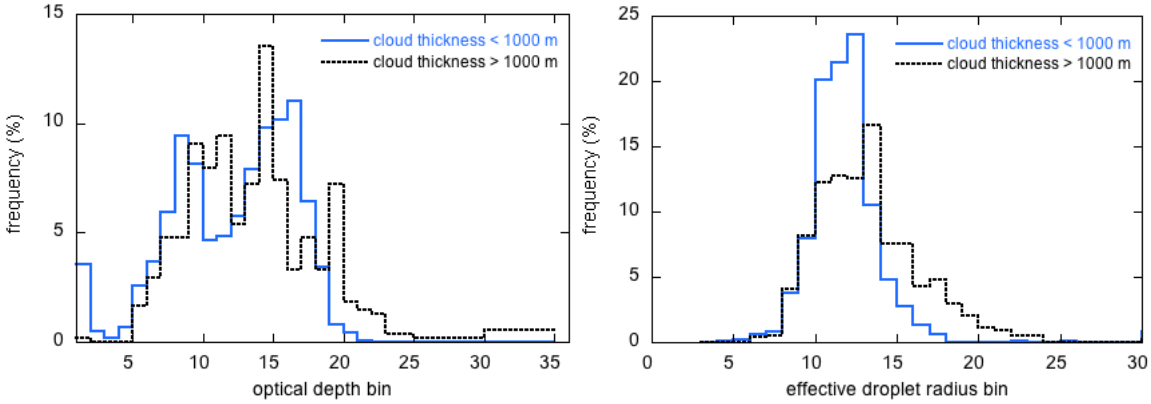

Figure 3. Frequency distribution of retrieved cloud optical depth τ_c (left) and cloud droplet effective radius (right) for all liquid water clouds sampled during the ISDAC time period of April – May 2008. Cloud-base heights are < 1000 m, and maximum cloud thickness is 3000 m.

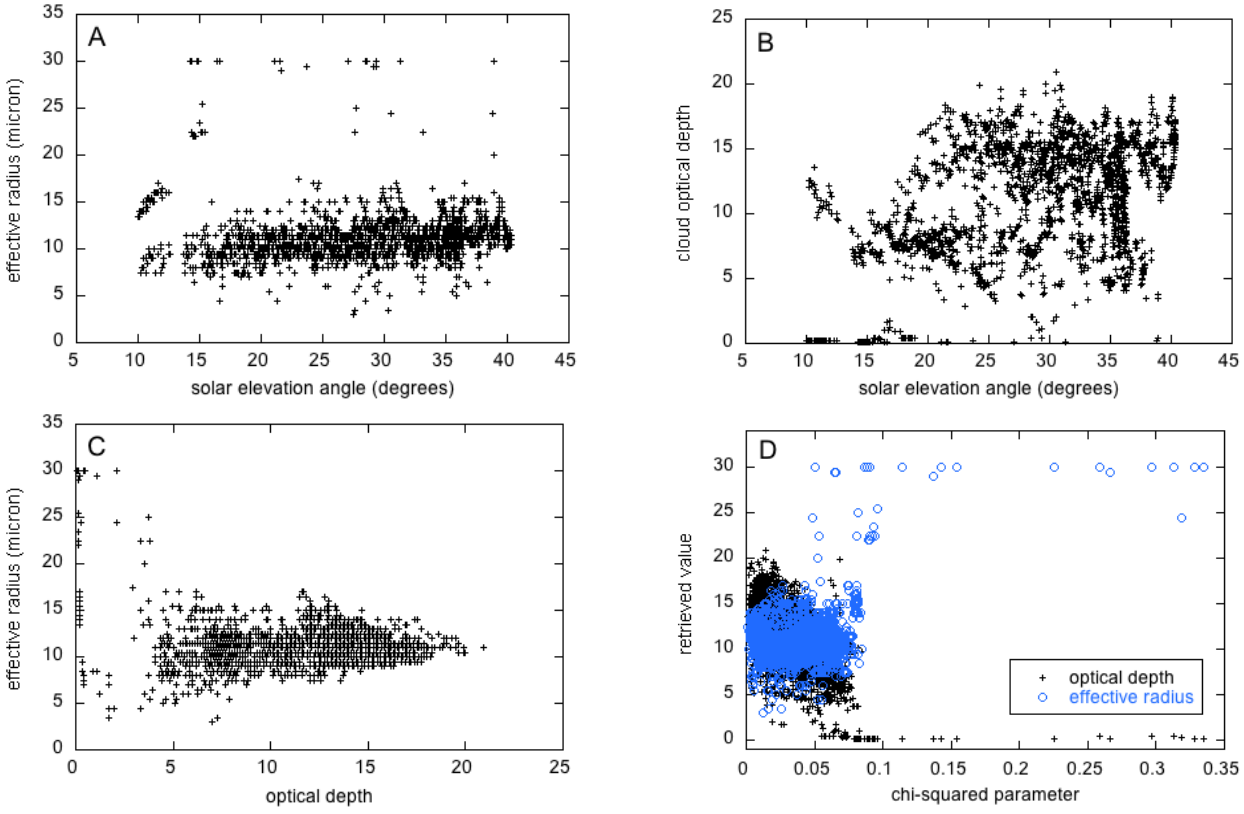

Figure 4. Demonstration of stability in the radiative transfer retrieval algorithm applied to ISDAC data; (A) lack of dependency in retrieved r_e on solar elevation angle, (B) lack of dependency in retrieved τ_c on solar elevation angle, (C) lack of dependency of retrieved r_e and τ_c upon each other, (D) identification of spurious large r_e values by means of their poorer least-squares fitting parameter.

aligned such that it is collinear with the optical axis, which is defined by the center of the lamp's filament and the center of the diffuser of the test instrument. By holding a mirror flush against the shadow ring of the instrument's collector and observing the retro-reflection of the laser beam, it is ensured that the instrument is aligned perpendicular to the optical axis when the rotary table is in the 0° position. The uncertainty of the 0° position was 0.06° for both azimuthal orientations. The DRT is enclosed with black curtains selected for low reflectivity. A black wall is installed approximately halfway between lamp and the test instrument. The wall has an aperture where it intersects the optical axis. The diameter of the aperture is selected such that the complete diffuser is illuminated under all conditions, but yet small enough to reduce stray light in the test compartment to an insignificant amount. The collector was tested at two azimuth orientation. The first measurement was at an azimuth angle of 0° and the second one at 90°. The orientation of the instrument for various settings of the rotary table and azimuth angles is illustrated in Figure 5.

For each instrument and azimuth orientation, the "cosine error" $f_2(\varepsilon,\varphi)$ of the instrument is calculated as:

$$f_2(\varepsilon,\varphi) = \frac{Y_{reading}(\varepsilon,\varphi)}{Y_{reading}(\varepsilon = 0°)\ \cos(\varepsilon)} - 1$$

where ε is the incidence angle of the radiation (equal to the angle of the rotary stage), φ is the azimuth angle of the instrument, and $Y_{reading}(\varepsilon,\varphi)$ is the dark-corrected reading of the radiometer at angles ε and φ. $Y_{reading}(\varepsilon = 0°)\ \cos(\varepsilon)$ is the ideal angular response, that is, the reading of the radiometer is proportional to the cosine of ε. For an ideal instrument, $f_2(\varepsilon,\varphi)$ is zero at all angles ε and φ.

Figure 6 shows the cosine error of the ASD collector for an azimuth angle of 0°. Data for $|\varepsilon| > 60°$ are from Series 2 and 3. There are gaps at zenith angles of -75°, -55°, and 55°. Measurements at those angles were in error, likely because a spectrum had been taken before the table was in the correct position. Measurements at 350 nm are close to the noise limit and show larger variations than measurements in the visible. Measurements beyond 2,200 nm are also close to the noise level, as the diffusing optic does not transmit well beyond this wavelength. Cosine errors at negative zenith angles tend to be smaller than at positive zenith angles. This asymmetry cannot be explained with the small angular uncertainty of the rotary table and must be caused by the collector and/or

the fiber coupling to the ASD spectrometer. The data shown in Figure 6 form the basis for a correction to the measured irradiance under cloud-free conditions.

A manuscript based on this BSI laboratory work is in preparation for the *Journal of Atmospheric and Oceanic Technology* (Lubin et al., 2013). In addition, this clear-sky correction will be added to the ARM archive of ISDAC data for the ASD shortwave spectroradiometer data.

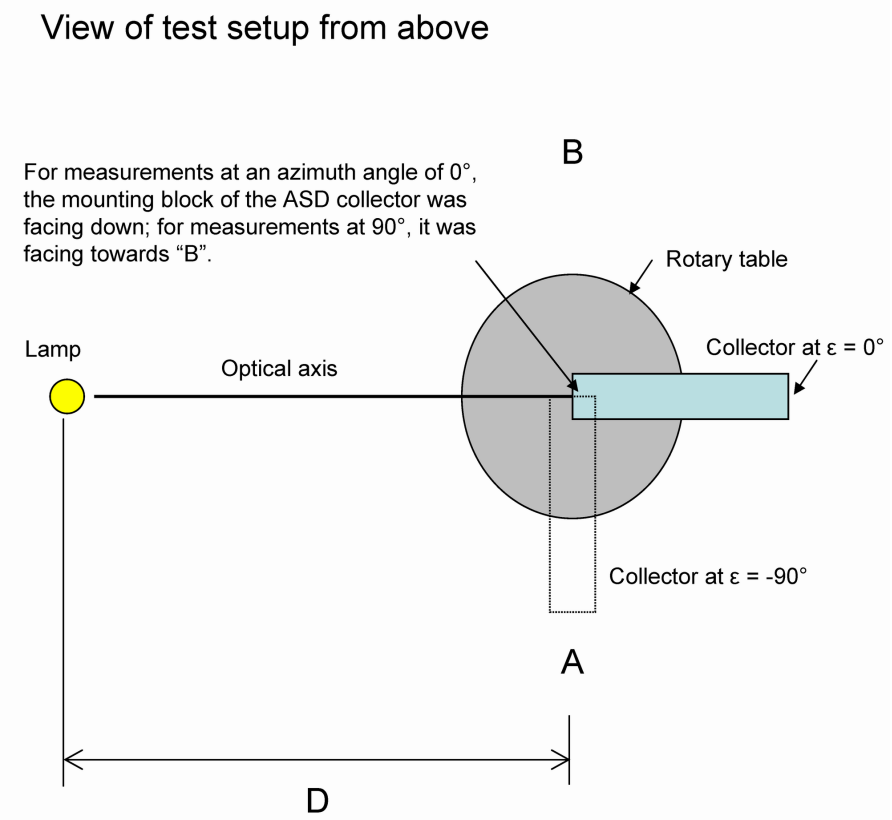

Figure 5. Sketch of test setup as seen from above. The collector of the ASD is mounted on a rotary table with the front surface of its diffuser tangent to the axis of rotation of the rotary table. At an incidence angle of ε =0°, the diffuser is perpendicular to the optical axis. At ε = –90°, the collector faces point B. At ε = +90° (not shown), the instrument faces point A. For an azimuth angle of 0°, the mounting block of the ASD collector was facing down; for measurements at 90° it was facing towards point B. The lamp is mounted at a distance of D from the axis of rotation of the rotary table.

Finally, during the first three months of this project we completed and published a manuscript in *Tellus-B*, which reports on how we utilized several years of NSA data to estimate the total (shortwave plus longwave) first indirect effect of aerosol in the springtime Arctic. This analysis also yielded surprising summertime evidence of aerosol indirect effects, possibly linked to dimetyhl sulfide (DMS) production in the open Arctic Ocean (Lubin and Vogelmann, 2010).

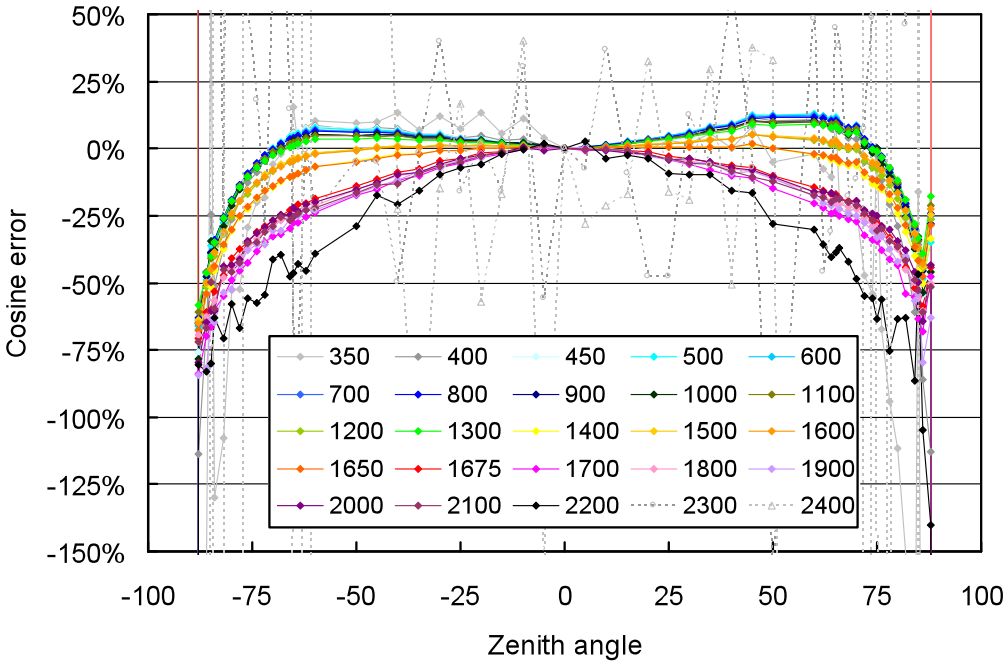

Figure 6. Cosine error of ASD collector for measurements at an azimuth angle of 0°. The legend indicates wavelength in nanometers.

Preliminary results from the Arctic modeling part of this project were presented in July 2012 at the ICCP in Leipzig. The poster from this presentation is attached below as Figure 7.

Studies of Cloud Microphysics in Arctic Mixed-Phase Cloud: Long ARM Data Time-Series Take Us Beyond Case Studies

16th International Conference on Clouds and Precipitation

J. Mülmenstädt,[1] D. Lubin,[1] L.M. Russell[1] and A.M. Vogelmann[2]

[1] Scripps Institution of Oceanography, [2] Brookhaven National Laboratory

Arctic clouds present an ongoing challenge

Predictions of Arctic climate change are sensitive to the radiative properties of clouds. However, Arctic clouds have complicated thermodynamic properties: mixed-phase cloud layers (MPC) with unexpectedly long persistence are common, and liquid water is present in clouds as cold as −40°C (e.g., Intrieri et al., 2002). Because of the complex dynamical and microphysical processes that are responsible for the persistence of MPC, current climate models have difficulty reproducing observed conditions (Morrison et al., 2012).

Correct parametrization of ice microphysics is crucial to model success in Arctic clouds because of the dependence of the surface radiation budget on the partitioning between liquid and ice cloud water. In recent years, multi-moment microphysics models have become available, which are prognostic in both particle number and mixing ratio (two "moments" of the particle size distribution) for several hydrometeor species. It is generally observed [e.g. in the two-part model intercomparison experiment performed by Klein et al. (2009) and Morrison et al. (2009)] that the multi-moment models lead to better agreement with observations than single-moment models under the same conditions. Nevertheless, large discrepancies between model results and observations are still common. The results of Klein et al. (2009) and Morrison et al. (2009) also suggest that model success is highly dependent on meteorological regime.

Using ARM data for model evaluation

Model performance is assessed by comparison to observations. Typically the observations come from field campaigns, but these campaigns are often short and not representative of the range of conditions encountered over longer time periods.

The Department of Energy (DOE) Atmospheric Radiation Measurement (ARM) program maintains a site in Barrow on the North Slope of Alaska (NSA) specifically to address the shortage of cloud observations in the Arctic and test and improve cloud parametrizations in models (Curry et al., 1996; Stamnes et al., 1999). As a result, there is now over a decade of near-continuous data available that includes a wealth of cloud-property measurements, including information on ice and liquid water content that is of great relevance to the cloud-modeling difficulties described above. Why has the full time-series of this data not been used in modeling studies so far? From the modeling standpoint, the observations extend over too much meteorological phase space. Before they can be used, they need to be reduced to a manageable number of meteorologically meaningful test cases.

Climatology of Barrow

At a latitude above 71° N, Barrow is the northernmost point in Alaska. It exhibits climatic features of maritime Arctic and polar desert, depending on season and meteorological regime. Mixed-phase clouds occur year-round except during the peak of summer. About 40% of mixed-phase clouds are multi-layer (Shupe, 2007). This makes Barrow a perfect cloud laboratory. Instrumentation at the ARM site includes surface meteorology, LIDARs, RADARs and radiometers.

Acknowledgments

This work was funded by the Department of Energy. Data was obtained from the U.S. DOE ARM Program; the Computational and Information Systems Laboratory at the National Center for Atmospheric Research; and the NOAA Earth System Research Laboratory Physical Science Division. Computing resources were provided by the Open Science Grid. We thank Mike Jensen for informative discussions about Microbase.

Works cited

Clothiaux, E. E., T. P. Ackerman, G. G. Mace, K. P. Moran, R. T. Marchand, M. A. Miller, and B. E. Martner, 2000: *J. Appl. Meteorol.*, **39 (5)**.

Curry, J. A., W. B. Rossow, D. Randall, and J. L. Schramm, 1996: *J. Clim.*, **9 (8)**.

Intrieri, J. M., M. D. Shupe, T. Uttal, and B. J. McCarty, 2002: *J. Geophys. Res.–Oceans*, **107 (C10)**.

Klein, S. A., et al., 2009: *Q. J. R. Meteorol. Soc.*, **135 (641)**.

Lin, Y.-H., R. Farley, and H. Orville, 1983: *J. Clim. App. Met.*, **22 (6)**.

Morrison, H., G. de Boer, G. Feingold, J. Harrington, M. D. Shupe, and K. Sulia, 2012: *Nature Geosci.*, **5 (1)**.

Morrison, H., G. Thompson, and V. Tatarskii, 2009a: *Mon. Weather Rev.*, **137 (3)**.

Morrison, H., et al., 2009: *Q. J. R. Meteorol. Soc.*, **135 (641)**.

Mülmenstädt, J., D. Lubin, L. Russell, and A. M. Vogelmann, 2012: *J. Climate*, (in press, doi:10.1175/JCLI-D-11-00636.1).

Shupe, M. D., 2007: *Geophys. Res. Lett.*, **34 (22)**.

Stamnes, K., R. G. Ellingson, J. A. Curry, J. E. Walsh, and B. D. Zak, 1999: *J. Clim.*, **12 (1)**.

Zhao, C., et al., 2012: *J. Geophys. Res.*, (in revision).

Classification by meteorological regime

The aim of our approach is to divide the observations into ensembles with similar meteorology. Each ensemble can be used as a test case for climate models. The classification is based on an automated objective clustering algorithm (k-means) and local surface meteorology (air temperature, surface pressure, relative humidity, wind). This work (Mülmenstädt et al., 2012) is the first objective meteorological classification performed in an Arctic setting.

Local meteorological regimes

Cluster	Frequency	Temp anomaly	Pressure	Rel hum anomaly	Wind speed	Wind dir
1	900	low	high	dry	average	NE
2	698	average	low	dry	average	S
3	1068	average	low	humid	high	NE
4	587	high	average	humid	average	NW

Column-integrated cloud and radiative properties differ between the categories

The following table lists column-integrated cloud and radiative properties that differ significantly ($p < 10^{-5}$ in a Kolmogorov-Smirnov test) between cluster pairs:

Cluster	1	2	3	4
1		Cloud base (C, M, L) Cloud cover PWV, LWP, IWP DLW CN	Cloud base (C, L) Cloud cover PWV, LWP, IWP DLW	Cloud base (C, M, L) Cloud cover PWV, LWP, IWP DLW CN
2	Cloud base (C, M, L) Cloud cover PWV, LWP, IWP DLW CN		Cloud base (M) PWV DLW CN	PWV, LWP DLW
3	Cloud base (C, L) Cloud cover PWV, LWP, IWP DLW	Cloud base (M) PWV DLW CN		Cloud base (M, L) PWV, LWP DLW CN
4	Cloud base (C, M, L) Cloud cover PWV, LWP, IWP DLW CN	PWV, LWP DLW	Cloud base (M, L) PWV, LWP DLW CN	

Cloud profiles differ between the categories

The ARSCL and Microbase multi-sensor products show large differences in vertical cloud profiles between clusters. (Clothiaux et al., 2000; Zhao et al., 2012)

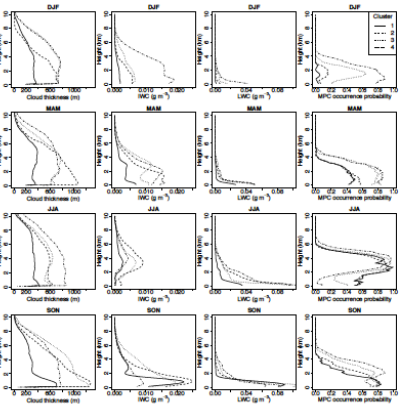

Reanalysis synoptic fields explain the local conditions

Composite NCEP/NCAR Reanalysis maps of each meteorological category can explain the observed cloud properties through synoptic meteorology or local thermodynamics.

Cluster 1: Anticyclonic flow of cold, dry polar air

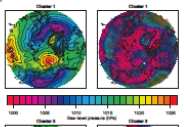

Cluster 2: Cyclonic flow of cold, dry polar air

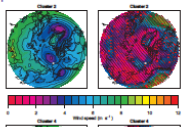

Cluster 3: Strong easterly winds, advection of mid-level maritime air

Cluster 4: Very moist maritime air in cyclonic flow through Bering Strait

Can meteorological regimes be used as model test cases?

The meteorological classification reduces 11 years of observations to four model test cases with similar meteorology. Because of the large number of days in each category, we can draw statistically robust conclusions about model performance. We will now use a regional model to test whether the classification in the previous section can pinpoint conditions where a model fails.

Regional model setup (WRF V3.3.1 centered on Barrow)

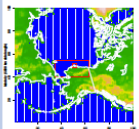

- 50 km, 10 km, 2 km nested grids
- 200 m vertical layers to 2 km height
- NCEP GFS/FNL initialization for 72 h run (24 h model spin-up)
- Two microphysical schemes considered:
  - Single-moment with ice, snow, graupel (Lin et al., 1983)
  - Double-moment ice, snow, rain and graupel (Morrison et al., 2009a)

DLW spread varies with meteorological regime

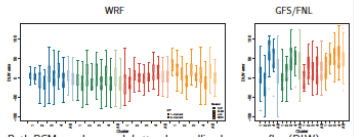

Both RCMs produce much better downwelling long-wave flux (DLW) agreement with observation than GFS. The model error spread varies greatly between clusters and seasons. The difference between single- and double-moment microphysics is consistent between seasons and clusters, giving it added statistical robustness.

Liquid- and Ice-water vertical profiles

Across all seasons and clusters, the double-moment scheme produces more liquid and ice water than the single-moment scheme:

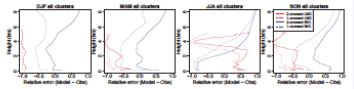

Within each season, there is also large variation between clusters:

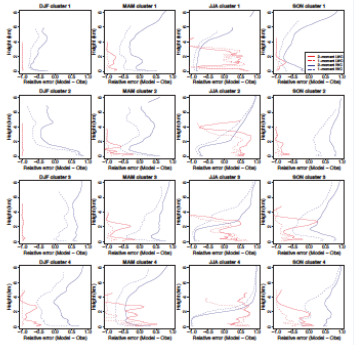

Meteorological classification permits conclusions about model performance

- In very cold or very warm conditions, liquid water does not depend on microphysics, but ice water still does
- Liquid is underestimated in the cold seasons and overestimated in JJA
- Double-moment microphysics produces good mid-altitude LWC in those regimes with warm advection in the midlevels
- Ice is overproduced in the double-moment scheme in SON (open water?), underproduced in JJA, otherwise close to observations
- When there is thick low cloud, ice tends to be overproduced

Summary

Large model uncertainties associated with mixed-phase clouds in the Arctic make it desirable to use long time series of cloud observations for model studies and improvement. We have assembled ensembles of similar meteorological conditions for model evaluation. Comparing models to observations separately for each category exposes models to the range of conditions found in nature. Intercomparison between the NCEP FNL operational model and WRF with two microphysical schemes demonstrates the utility of this approach.

J. Mülmenstädt Mail: Scripps Institution of Oceanography San Diego CA 92093-0221 Email: jmuelmen@ucsd.edu WWW: http://aerosols.ucsd.edu

Figure 7. Poster presented at the *International Conference on Clouds and Precipitation* in Leipzig, Germany, in July 2012 by Johannes Mülmenstädt, showing preliminary results from Mülmenstädt et al. (2013).

6. Products developed under the award: Publications, conference papers, or other public releases of results.

Publications

Lubin, D., and A. M. Vogelmann, 2010: Observational quantification of a shortwave aerosol indirect effect in the Arctic. *Tellus-B*, **62**, 181-189.

Lubin, D., and A. M. Vogelmann, 2011: The influence of mixed-phase clouds on surface shortwave irradiance during the Arctic spring. *Journal of Geophysical Research*, **116**, doi:10.1029/2011JD015761.

Lubin, D., and A. M. Vogelmann, 2013: Retrieval of Arctic liquid water cloud radiative properties from shortwave spectroradiometer data during ISDAC. *Journal of Atmospheric and Oceanic Technology,* in preparation.

Lubin, D., G. Bernhard, R. Scott, and A. M. Vogelmann, 2013: Cosine response characterization of an ultraviolet through near-infrared wavelength spectroradiometer: Application to the ASD FieldSpec series. *Journal of Atmospheric and Oceanic Technology*, in preparation.

Mülmenstädt, J., D. Lubin, L. M. Russell, and A. M. Vogelmann, 2012: Cloud properties over the North Slope of Alaska: Identifying the prevailing meteorological regimes. *Journal of Climate*, **25**, 8238-8258.

Mülmenstädt, J., D. Lubin, L. M. Russell, and A. M. Vogelmann, 2013: Cloud properties over the North Slope of Alaska: Comparison of microphysical simulations with ensemble data in the prevailing meteorological regimes. *Journal of Climate*, in preparation.

Conference papers

Mülmenstädt, J., D. Lubin, L. M. Russell, and A. M. Vogelmann, 2013: Studies of Cloud Microphysics in Arctic Mixed-Phase Cloud: Long ARM Data Time-Series Take Us Beyond Case Studies. Leipzig, Germany, July 2012. *International Conference on Clouds and Precipitation.*

7. For projects involving computer modeling:

a. Model description, key assumptions, version, source and intended use
This project used one regional model: the Weather Research and Forecasting Model with Chemistry version 3.1 (WRF-Chem). This model is uncontroversial, widely validated research tools with proven track records in the literature. WRF is a regional numerical weather prediction model developed through a multi-institutional endeavor headed at NCAR and is used for both forecasting and climate research applications. WRF-Chem is a modified version of the WRF model, which includes online chemistry, capable of simulating aerosol-cloud-radiation direct and indirect interactions at cloud-resolving scales. The chemistry component of the WRF model is described by *Grell et al.* [2005] and *Fast et al.* [2006].

b. Performance criteria for the model related to the intended use
WRF-Chem has been validated throughout its development (WRF-Chem: *Grell et al.* [2005][1], *Fast et al.* [2006]).

c. Test results to demonstrate the model performance criteria were met
The primary reference for our new test results is:
Mülmenstädt, J., D. Lubin, L. M. Russell, and A. M. Vogelmann, 2013: Cloud properties over the North Slope of Alaska: Comparison of microphysical simulations with ensemble data in the prevailing meteorological regimes. *Journal of Climate*, in preparation.

d. Theory behind the model, expressed in non-mathematical terms
Regional climate modeling studies provide high-resolution trajectory, aerosol, and cloud details in a particular region.

e. Mathematics to be used, including formulas and calculation methods
For mathematical details regarding individual model subcomponents see *Grell et al.* [2005] for WRF-Chem.
f. Whether or not the theory and mathematical algorithms were peer reviewed, and, if so, include a summary of theoretical strengths and weaknesses
The model has been extensively peer reviewed. An ongoing list of select publications for each model can be found at: WRF (http://ruc.noaa.gov/wrf/WG11/References/WRF-Chem.references_July2012.htm).

g. Hardware requirements
The model can be run on a variety of platforms, as described at http://www.wrf-model.org.

h. Documentation (e.g., user guide, model code)
The WRF user guide and model code can be found at http://www.wrf-model.org.

References Cited

Fast JD, WI Gustafson Jr., RC Easter, RA Zaveri, JC Barnard, EG Chapman, and GA Grell. 2006. Evolution of ozone, particulates, and aerosol direct forcing in an urban area using a new fully-coupled meteorology, chemistry, and aerosol model. J. Geophys. Res., 111:D21305.

Grell GA, SE Peckham, R Schmitz, and SA McKeen, G Frost, WC Skamarock, and B Eder. 2005. Fully coupled 'online' chemistry in the WRF model. Atmos. Environ., 39:6957-6976.